

State Space Modeling of Dimensional Variation Propagation in Multistage Machining Process Using Differential Motion Vectors

Shiyu Zhou, Qiang Huang, and Jianjun Shi

Abstract—In this paper, a state space model is developed to describe the dimensional variation propagation of multistage machining processes. A complicated machining system usually contains multiple stages. When the workpiece passes through multiple stages, machining errors at each stage will be accumulated and transformed onto the workpiece. Differential motion vector, a concept from the robotics field, is used in this model as the state vector to represent the geometric deviation of the workpiece. The deviation accumulation and transformation are quantitatively described by the state transition in the state space model. A systematic procedure that builds the model is presented and an experimental validation is also conducted. The validation result is satisfactory. This model has great potential to be applied to fault diagnosis and process design evaluation for complicated machining processes.

Index Terms—Differential motion vector, multistage machining process, state space model, variation propagation.

NOMENCLATURE

${}^0\text{FCS}, \text{FCS}$	Nominal and actual fixture coordinate system.
HTM	Homogeneous transformation matrix.
$H_n^R, {}^0H_n^R$	Actual and nominal HTM between RCS and LCS_n .
δH_n^R	Deviation HTM defined by \mathbf{d}_n^R and θ_n^R .
$I_{n \times n}, O_{m \times n}$	n by n identity matrix and m by n zero matrix, respectively.
LCS_i	i th local coordinate system.
M, N	Total number of key features and machining stages, respectively.
RCS	Reference coordinate system.
$R_n^R, {}^0R_n^R$	Actual and nominal rotational matrix between RCS and LCS_n .
T_1, T_2	Transformation matrices for datum-induced error.
T_3	Transformation matrix for fixture error.

VD&T
 $\mathbf{d}_n^R, \theta_n^R$

$d_{nx}^R, d_{ny}^R, d_{nz}^R$

k

$l(k)$

$\mathbf{n}, \mathbf{o}, \mathbf{a}$

$\tilde{\mathbf{p}}$

$\tilde{\mathbf{p}}$

$q_i(k)$

$r_i(k)$

$s_i(k)$

$\mathbf{t}_n^R, {}^0\mathbf{t}_n^R$

$t_{nx}^R, t_{ny}^R, t_{nz}^R$
 \mathbf{x}_n^R

$\mathbf{x}(k)$

$\mathbf{x}^n(k)$

$\Delta_n^R, \bar{\Delta}_n^R$

$\omega_n^R, {}^0\omega_n^R$

$\theta_{nx}^R, \theta_{ny}^R, \theta_{nz}^R$

$[\cdot]_{(n)}$

\times

Vectorial dimensioning and tolerancing.

Position and orientation deviation of LCS_n from nominal positions w.r.t. RCS.

Three elements of \mathbf{d}_n^R .

Stage index, $k = 1 \dots N$.

Total number of newly generated feature at stage k .

Column vectors of a rotational matrix.

Skew symmetric matrix obtained from vector \mathbf{p} .

Extension of a vector \mathbf{p} . $\tilde{\mathbf{p}} = [\mathbf{p}^T \ 1]^T$.

Feature index for newly generated feature at stage k . $i = 1 \dots l(k)$.

Feature index for the primary datum ($i = 1$), secondary datum ($i = 2$), and tertiary datum ($i = 3$) of the k th stage.

Feature index for the generated feature up to stage k (not include stage k). i is an integer from 1 to total number of generated features up to stage k .

Actual and nominal vector of the origin of LCS_n expressed in RCS.

Three elements of \mathbf{t}_n^R .

Differential motion vector representing the deviation of LCS_n in RCS. It is a stack of \mathbf{d}_n^R and θ_n^R and is expressed in LCS_n .

State vector.

Stack of differential motion vectors of newly generated features at stage k .

Differential transformation matrix corresponding to δH_n^R and $(\delta H_n^R)^{-1}$.

Actual and nominal Euler rotational angles between RCS and LCS_n .

Three elements of θ_n^R .

n th element of a vector in the bracket.

Cross product of two vectors.

Manuscript received July 23, 2001; revised April 15, 2002. This paper was recommended for publication by Associate Editor M. Wang and Editor N. Viswanadham upon evaluation of the reviewers' comments. This work was supported by the National Science Foundation Engineering Research Center for Reconfigurable Machining Systems under Grant EEC95-92125 at the University of Michigan, and the valuable input from the Center's industrial partners.

S. Zhou is with the Department of Industrial Engineering, University of Wisconsin, Madison, WI53706, USA (e-mail: szhou@engr.wisc.edu).

Q. Huang and J. Shi are with the Department of Industrial and Operations Engineering, University of Michigan, Ann Arbor, MI 48109 USA (e-mail: huangq@umich.edu; shihang@umich.edu).

Digital Object Identifier 10.1109/TRA.2003.808852

I. INTRODUCTION

PRODUCT variation reduction is an important engineering objective in both design and manufacturing. For a multistage machining process, the product variation at certain stages consists of two components: the variation brought by the volumetric error of the current machine stage and the variation brought by the datum feature error produced from previous stages. The second component exists because we have to use

part features produced by previous stages as the machining datum in current operation. The variation from previous stages will be accumulated onto current operation.

At each single stage, there are many types of volumetric error sources, such as the geometric and kinematic errors, thermal errors, cutting force induced errors, and fixturing errors. A huge body of literature can be found on the error modeling and compensation on a single machining stage. A review of these papers can be found in Ramesh *et al.* [1], [2]. However, due to the complicated interactions between different variation errors at different stages, very few attempts have been made on the variation propagation analysis for a multistage machining process. Mantripragada and Whitney [3] adopted the concept of output controllability from control theory to evaluate and improve the automotive body structure design. Lawless *et al.* [4] and Agrawal *et al.* [5] investigated variation transmission in both assembly and machining process by using an AR(1) model. Jin and Shi [6] proposed a state space model to depict the variation propagation in a multistage body assembly process. Their approach cannot be applied directly to machining processes. Huang *et al.* [7] proposed a variation propagation model for multistage machining process. However, that model is an implicit nonlinear model. Djurdjanovic and Ni [8] extended Huang's formulation to obtain a linear model. In their derivation, a norm vector and a position vector are used to represent the geometric error of the workpiece and Taylor series expansion is used to linearize the model. Although the final model is in linear form, the explicit expression of each system matrix is not given. The physical insights we can obtain are limited.

In this paper, an explicit analytical variation propagation model is developed for a multistage machining process. This model is in the state space form. Differential motion vector, a concept widely used in robotics [9], is used as the state vector to describe the workpiece geometric deviation. The theory of homogeneous transformation is heavily used in the derivation and explicit expressions for all the system matrices are given. The process and production information are quantitatively integrated together in the system matrices of this model. This model can be used for process evaluation in design and root cause identification in manufacturing for multistage machining processes.

The terminologies, representations of part features, and assumptions of this model are introduced in Section II. The model itself is derived in Section III. Section IV presents the experimental validation results for this model. Finally, the conclusions and some discussion of the applications of this model are given in Section V.

II. WORKPIECE GEOMETRIC DEVIATION REPRESENTATION AND MODEL ASSUMPTIONS

A machining process is used to remove materials from the workpiece to obtain higher dimensional accuracy, better surface finishing, or a more complicated surface form which cannot be obtained by other processes. A complicated machining process is usually a "multistage" machining process, which refers to a

machining process where a part will be machined through different setups when it passes through this process. It is not necessary that a multistage machining process contains multiple machining stations. If there are different setups on only one machining station, this machining process is still considered as a multistage machining process.

When a workpiece passes through certain stage of a multistage machining process, the machining error and fixturing error of this stage will be accumulated on the workpiece. These errors will again affect the machining accuracy of the following stages if the datum used by following stage is produced at current stage. Since the workpiece carries all the machining error information, a representation of accuracy of a workpiece is required to study the complicated interaction of errors among different stages.

A. Workpiece Geometric Deviation Representation

To regulate the deviations of part features, researchers have developed standards for geometric dimensioning and tolerancing (ISO 1101 (1983) or ANSI Y14.5(1982)). However, these conventional geometric tolerances are originated from the hard gauging practice. They are not suitable for the working principle of Coordinate Measurement Machine (CMM) that is now a standard measurement equipment for machining process. In addition, the representation of part feature in the conventional geometric tolerances does not conform to the part representations used in CAD/CAM systems.

Recently, some researchers [10] proposed a vectorial dimensioning (VD&T) strategy. The principle of VD&T is based on the concept of substitute elements or substitute. A substitute feature is an imaginary geometrical ideal feature (e.g., plane, circle, line) whose location, orientation, and size (if applicable) are calculated from the measurement data points of the workpiece surface. Substitute features are represented by the location vector, orientation vector, and size(s). The location vector indicates the location of a specified point of the substitute feature. The substitute orientation vector is a unit vector that is normal to the substitute plane or parallel to the substitute axis (cylinder, cone, etc). The size is available for some features. For example, the diameter is the size of a circular hole. The VD&T workpiece feature representation follows the working principle of CMM and CAD/CAM systems. The measurement data from CMM can be analyzed and compared with the design model directly. The difference between the true feature and the design requirement can be feedback to the manufacturing process directly. It is a better tolerancing method for manufacturing process control [11].

In this paper, we adopt a vectorial feature representation proposed by Yau [12], [13]. The difference between his representation and the ordinary vectorial representation is in the orientation representation. Instead of using a unit direction vector, he used a vector that consists of three Euler rotating angles to represent the orientation of the substitute feature. The representation of using unit direction vector makes it difficult to designate tolerance on the orientation for a general 3-D geometric element. Moreover, the direction vector representation violates certain functional requirements that VD&T intends to capture. Another advantage of angular representation of orientation is that there are many mathematical tools available in the fields

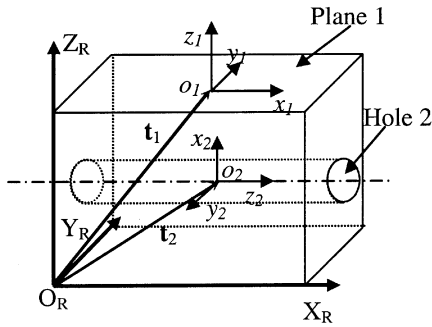


Fig. 1. Illustration of feature representation.

of robotics and kinematics for this representation. Therefore, in this paper, a location vector and a vector that consists of three rotating Euler angles are used to represent a workpiece feature. Since the size of a feature is usually formed at one machining stage, it is not considered in the following derivation.

The part representation is illustrated in Fig. 1. $O_R X_R Y_R Z_R$ is the reference coordinate system (RCS). Plane 1 and Hole 2 are represented by the local coordinate systems (LCSs) that are attached on them, respectively. The position and orientation of Plane 1 can be represented by $[t_1^T \omega_1^T]^T$. t_1 is the location vector that points to the origin of LCS_1 . ω_1^T is a vector contains roll, pitch, and yaw Euler rotating angles between coordinate system LCS_1 and RCS. ω_1^T is $[0 \ 0 \ 0]^T$ in Fig. 1. Similarly, Hole 2 can be represented by $[t_2^T \omega_2^T]^T$. ω_2^T is $[0 \ \pi/2 \ \pi]^T$ in Fig. 1.

To describe the accuracy of a machined workpiece, we need to study the relationships between different features. Since LCS is used to represent each feature, the relationships among different features can be described by the relationships of corresponding coordinate systems. Homogeneous transformation matrix (HTM) as a mathematical tool is used to study the transformation between different coordinate systems. Appendix I listed the basic notation and results of HTM used in this paper.

If the feature index is i , we denote the corresponding LCS as LCS_i . The deviation of the feature is described by the deviation of the corresponding actual LCS from the corresponding nominal LCS. As shown in Appendix I, the deviation of a LCS can be represented by a differential motion vector $\mathbf{x}_n^R = [\mathbf{d}_n^R]$. If the actual location vector for the n th element is \mathbf{t}_n^R and the corresponding nominal location vector is ${}^0\mathbf{t}_n^R$, then $\mathbf{t}_n^R = {}^0\mathbf{t}_n^R + \mathbf{d}_n^R$. However, the orientation vector does not have this property, i.e., in general, $\omega_n^R \neq {}^0\omega_n^R + \theta_n^R$. The reason is that the multiplication of rotating matrix does not commute in general cases.

In summary, a location vector and an orientation angular vector are used in this paper to represent a feature in the RCS. The relative position and orientation of a feature is described as a homogenous transformation matrix. The deviation of a feature from its nominal value is represented by a differential motion vector. The rationale of this representation is that it conforms with the working principles of CMM and CAD/CAM models. Moreover, many mathematical tools are available for analyzing this representation.

B. Model Assumptions

Based on the workpiece geometric deviation representation, a multistage machining process can be described by Fig. 2.

The workpiece deviation before stage k is represented by state vector $\mathbf{x}(k)$. $\mathbf{x}(k)$ is a stack of differential motion vectors of all key features of the workpiece. If there are M key features on a workpiece, the dimension of \mathbf{x} vector will be $6M$ by 1. Before the feature is produced, the corresponding differential motion vector is set to be zero. The initial value of state vector \mathbf{x} is zero before the first stage. After the workpiece passes the first stage, the differential motion vectors corresponding to the features produced at the first stage are set to be nonzero values as the dimensional deviations generated at the first stage. By this way, state vector $\mathbf{x}(2)$ is generated. Similarly, the state vector after the k th stage $\mathbf{x}(k+1)$ can be generated. The workpiece deviation at stage k comes from three sources: the datum-induced deviation caused in previous stages, the machining inaccuracy at the current stage, and unmodeled noise. The deviation propagation can be written in the following linear discrete state space format [14]:

$$\begin{aligned} \mathbf{x}(k+1) &= A(k)\mathbf{x}(k) + B(k)\mathbf{u}(k) + \mathbf{w}(k) \\ \mathbf{y}(k) &= C(k)\mathbf{x}(k) + \mathbf{v}(k) \end{aligned} \quad (1)$$

where $A(k)\mathbf{x}(k)$ represents the deviations of previously machined features and the deviation of newly machined features that is only contributed by the datum error, $B(k)\mathbf{u}(k)$ represents the workpiece deviation caused by the relative deviation between the workpiece and the cutting tool (this deviation is caused by the fixture error and the imperfection of the tool path), $\mathbf{y}(k)$ is the measurement, $\mathbf{w}(k)$ is the unmodeled system noise, and $\mathbf{v}(k)$ is the measurement noise. Two assumptions are implied in this formulation: 1) machining error on single stage is modeled as a tool path deviation from its nominal path and 2) only position and orientation error are considered. Profile error is not included.

The rationale of the first assumption is as follows. Many types of machining error sources can affect the accuracy of the workpiece on a single stage. According to Ramesh [1], they can be categorized as quasistatic errors and dynamic errors. Quasistatic errors are the static or slow varying errors between the tool and the workpiece. They include the geometric and kinematic errors, thermal errors, cutting force induced errors, tool wear induced error, fixturing error, etc. Quasi-static errors account for about 70% of overall machining errors. Dynamic errors are caused by sources such as spindle error, machine structure vibration, controller error, etc. They are more dependent on particular operating conditions of the machine. The state vector of this model is the manifestation of all machining error sources on the workpiece. It does not directly map to certain machining error. Using the homogeneous transformation representation of the feature deviation, all the position errors and orientation errors can be included in this model. The detailed modeling of certain machining errors for the whole working space of a machine stage is quite involved. For example, the geometric error that forms one of the largest sources of machining inaccuracy contains 21 interrelated error components for a three-axis machine. To simplify the problem, the machining error input to the model $\mathbf{u}(k)$ is represented as a deviation of the tool path from its nominal path. It is possible to map certain machining error components to the tool path deviation.

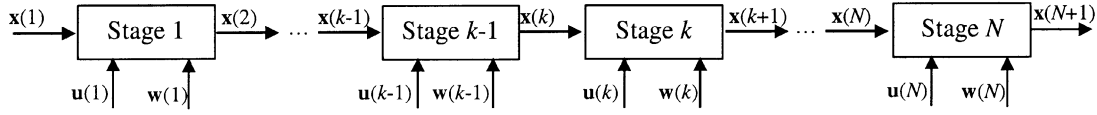


Fig. 2. Diagram of a multistage machining process.

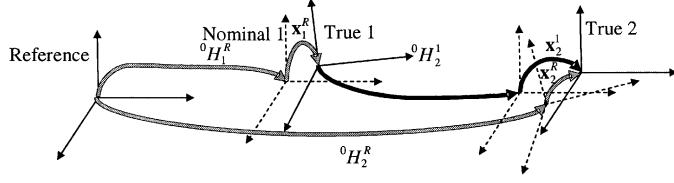


Fig. 3. Transition of differential motion vector: case 1.

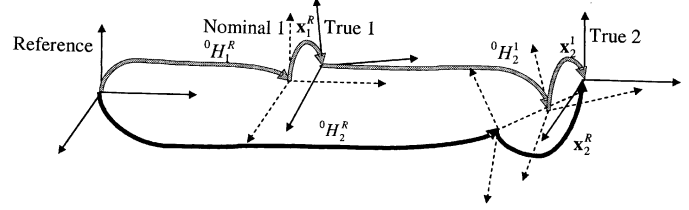


Fig. 4. Transition of differential motion vector: case 2.

The rationale for the second assumption is that this model focuses on describing the machining variation propagation among different stages. Since most the profile errors are generated on a single stage and keep unchanged throughout the whole process, it is not necessary to build a model describing its transformation and propagation. Therefore, profile errors are not included in this model.

III. DERIVATION OF THE STATE SPACE MODEL FOR MULTISTAGE MACHINING PROCESSES

To setup a state space model for the variation propagation in a multistage machining process, we need to find a general expression for the system matrices in (1). First, useful general properties of differential motion vector are introduced.

A. Properties of Differential Motion Vectors

One common scenario of transition of differential motion vectors is given in Fig. 3. In this case, we know the deviation of feature 1 w.r.t. the reference and the deviation of feature 2 w.r.t. feature 1, we want to calculate the deviation of feature 2 w.r.t. the reference. This problem is solved by Corollary 1. The proof is given in Appendix II.

Corollary 1: Consider a RCS and two features 1 and 2. Given ${}^0H_1^R$, ${}^0H_2^1$ and the deviation of feature 1 w.r.t. RCS, \mathbf{x}_1^R and the deviation of feature 2 w.r.t. feature 1, \mathbf{x}_2^1 , then

$$\mathbf{x}_2^R = \begin{bmatrix} ({}^0R_2^1)^T & -({}^0R_2^1)^T \cdot ({}^0\hat{\mathbf{t}}_2^1) & I_{3 \times 3} & 0 \\ 0 & ({}^0R_2^1)^T & 0 & I_{3 \times 3} \end{bmatrix} \begin{bmatrix} \mathbf{x}_1^R \\ \mathbf{x}_2^1 \end{bmatrix}. \quad (2)$$

Another important transition of differential motion vectors is shown in Fig. 4. In this transition, we know the deviation of feature 1 w.r.t. reference and the deviation of feature 2 w.r.t. reference, we want to calculate the deviation of feature 2 w.r.t. feature 1. This problem is solved in Corollary 2. The proof is also given in Appendix II.

Corollary 2: Consider a RCS and two features 1 and 2. Given ${}^0H_1^R$ and ${}^0H_2^R$ the deviation of feature 1 w.r.t. RCS, \mathbf{x}_1^R and the deviation of feature 2 w.r.t. RCS, \mathbf{x}_2^R , then

$$\mathbf{x}_2^1 = \begin{bmatrix} -({}^0R_2^1)^T & ({}^0R_2^1)^T \cdot ({}^0\hat{\mathbf{t}}_2^1) & I_{3 \times 3} & 0 \\ 0 & -({}^0R_2^1)^T & 0 & I_{3 \times 3} \end{bmatrix} \begin{bmatrix} \mathbf{x}_1^R \\ \mathbf{x}_2^R \end{bmatrix}. \quad (3)$$

These two corollaries are very useful when the RCS switches to another coordinate system.

B. Model Derivation

For the sake of convenience, the definitions of the four coordinate systems involved in the derivation are listed.

- 1) LCS represents the features of the workpiece.
- 2) RCS is the reference for the features of the workpiece. The primary datum feature, which is explained in following section, is often selected as RCS. RCS is also called ‘‘Part Coordinate System’’ in some literature.
- 3) Fixture Coordinate System (FCS) is determined by the actual fixture setup.
- 4) Nominal Fixture Coordinate System (0 FCS) is determined by the ideal fixture setup. FCS is also called ‘‘Machine Coordinate System’’ in some literature.

The state vector $\mathbf{x}(k)$ is defined as a stack of differential motion vectors corresponding to each feature w.r.t. RCS. It is clear that the reference feature does not have any deviation by definition. There are three major components in $\mathbf{x}(k)$:

- 1) Machining error, which is defined as the deviation of the cutting tool from its nominal path w.r.t. 0 FCS. Since the LCS of the newly generated feature is determined by the cutting tool path, the machining error can be represented by the deviation of LCS with respect to 0 FCS.
- 2) Fixturing error, which is caused by the imperfection of the locators. It is represented by the deviation of FCS with respect to 0 FCS.
- 3) Datum error, which is the deviation of FCS with respect to RCS.

The relationships among these coordinate systems and errors are shown in Fig. 5.

The machining error is represented by a differential motion vector that describes the deviation of LCS w.r.t. 0 FCS. It can be further decomposed into thermal, geometric error, and/or other machining errors sources. To limit the scope of this article, this part is not included here.

1) Analysis of Datum-Induced Error: The most commonly used fixture scheme in practice is the 3-2-1 fixturing scheme. A general 3-2-1 layout is shown in Fig. 6(a).

Surface ABCD defines the primary datum plane, which constrains two rotational and one translational motion. ADHE is the secondary datum plane, which constrains one rotational and one translational motion. CDHG is the tertiary datum plane, which constrains the last translational motion. They are represented

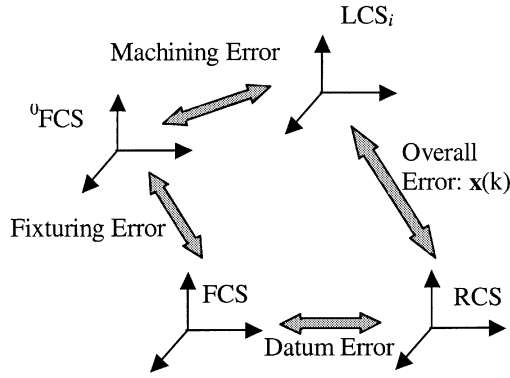
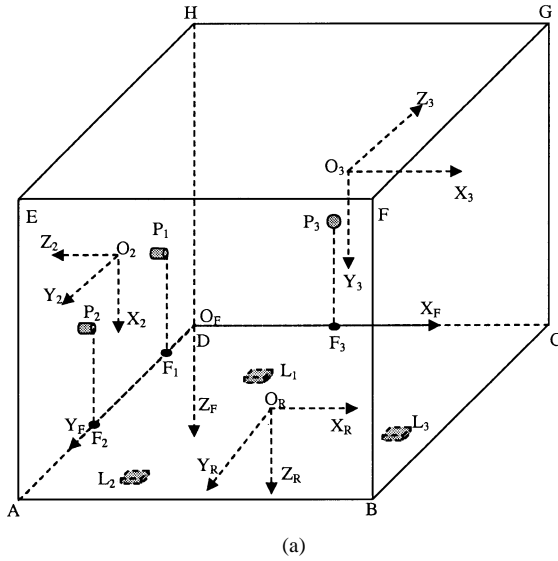
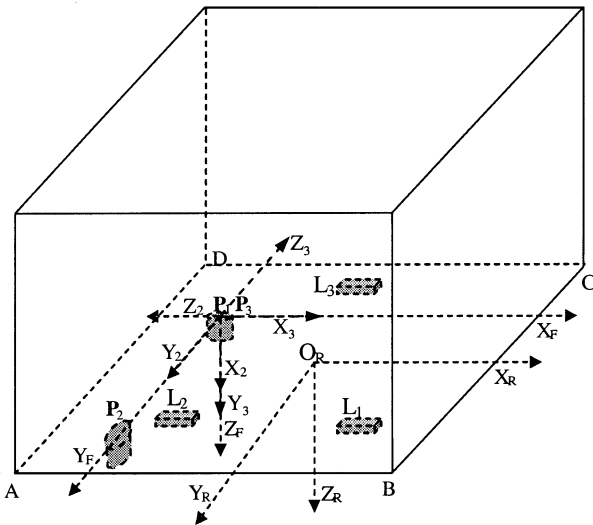


Fig. 5. Composition of overall feature deviation.



(a)



(b)

Fig. 6. 3-2-1 fixturing setup by a plane and three locators. (a) General 3-2-1 setup. (b) Variation of (a).

by LCS of $O_R X_R Y_R Z_R$, $O_2 X_2 Y_2 Z_2$, and $O_3 X_3 Y_3 Z_3$, respectively. F_1 , F_2 , and F_3 are the perpendicular projection points of the locators P_1 , P_2 , and P_3 on the primary datum. The fixture coordinate system (FCS) is shown in Fig. 6 as $O_F X_F Y_F Z_F$. $F_1 F_2$ is the Y axis of FCS, the line passing F_3 and perpendicular to

$F_1 F_2$ is the X axis of FCS, Z axis is perpendicular to the primary datum plane. The LCS of the primary datum plane (surface ABCD) is taken as the RCS. The secondary datum plane is denoted as feature 2 and its deviation is represented as x_2^R . The tertiary datum plane is denoted as feature 3 and its deviation is represented as x_3^R . Given x_2^R and x_3^R , the deviation of FCS w.r.t. RCS, x_F^R , can be obtained by

$$\mathbf{x}_F^R = T_1 \mathbf{x}_2^R + T_2 \mathbf{x}_3^R \quad (4)$$

where T_1 and T_2 are determined by the nominal positions of feature 2, 3, and the fixture locating pins. T_1 and T_2 can be obtained by the following general procedure.

Let \mathbf{p}_1 and \mathbf{p}_2 be the datum points touching the secondary datum and \mathbf{p}_3 be the datum point touching the tertiary datum. The nominal coordinates of these three points in FCS are denoted as \mathbf{p}_1^F , \mathbf{p}_2^F , and \mathbf{p}_3^F . Denoting $\tilde{\mathbf{p}} = [\mathbf{p}^T \ 1]^T$, we have

$$\begin{cases} H_R^2 H_F^R \tilde{\mathbf{p}}_1^F = \tilde{\mathbf{p}}_1^2 \\ H_R^2 H_F^R \tilde{\mathbf{p}}_2^F = \tilde{\mathbf{p}}_2^2 \\ H_R^3 H_F^R \tilde{\mathbf{p}}_3^F = \tilde{\mathbf{p}}_3^3 \end{cases} \quad (5)$$

To guarantee that these points touch with the corresponding part surface, the z coordinates of these points in LCS are zeros (the z direction is defined as the normal direction of the surface). Consider the first equation. Noting $H_R^2 = (H_2^R)^{-1} = ({}^0 H_2^R \delta H_2^R)^{-1} = (\delta H_2^R)^{-1} \cdot {}^0 H_2^R = (\bar{\Delta}_2^R + I) \cdot {}^0 H_2^R$ and $H_F^R = {}^0 H_F^R \cdot (\Delta_F^R + I)$, the left-hand side of the first equation of (5) changes to

$$\begin{aligned} (\bar{\Delta}_2^R + I) \cdot {}^0 H_2^R \cdot {}^0 H_F^R \cdot (\Delta_F^R + I) \tilde{\mathbf{p}}_1^F \\ \approx (\bar{\Delta}_2^R \cdot {}^0 H_F^2 + {}^0 H_F^2 \cdot \Delta_F^R + {}^0 H_F^2) \tilde{\mathbf{p}}_1^F. \end{aligned} \quad (6)$$

The third element of $\tilde{\mathbf{p}}_1^2$ is zero to guarantee touching, therefore

$$\left[(\bar{\Delta}_2^R \cdot {}^0 H_F^2 + {}^0 H_F^2 \cdot \Delta_F^R + {}^0 H_F^2) \tilde{\mathbf{p}}_1^F \right]_{(3)} = 0. \quad (7)$$

Under nominal conditions, \mathbf{p}_1 , \mathbf{p}_2 , and \mathbf{p}_3 should touch with datum plane. Hence, $[{}^0 H_F^2 \cdot \tilde{\mathbf{p}}_1^F]_{(3)} = 0$. Equation (7) changes to

$$\left[\Delta_2^R \cdot {}^0 H_F^2 \cdot \tilde{\mathbf{p}}_1^F \right]_{(3)} = \left[{}^0 H_F^2 \cdot \Delta_F^R \cdot \tilde{\mathbf{p}}_1^F \right]_{(3)}. \quad (8)$$

Denoting

$$\begin{aligned} \Delta_2^R &= \begin{bmatrix} \hat{\theta}_2^R & \mathbf{d}_2^R \\ \mathbf{0} & 0 \end{bmatrix} \\ {}^0 H_F^2 &= \begin{bmatrix} {}^0 \mathbf{n}_F^2 & {}^0 \mathbf{o}_F^2 & {}^0 \mathbf{a}_F^2 & {}^0 \mathbf{t}_F^2 \\ 0 & 0 & 0 & 1 \end{bmatrix} \end{aligned}$$

we have

$$\begin{aligned} \left[\Delta_2^R \cdot {}^0 H_F^2 \cdot \tilde{\mathbf{p}}_1^F \right]_{(3)} &= \left[\left[\theta_2^R \times {}^0 \mathbf{n}_F^2 \right]_{(3)} \left[\theta_2^R \times {}^0 \mathbf{o}_F^2 \right]_{(3)} \right. \\ &\quad \left. \left[\theta_2^R \times {}^0 \mathbf{a}_F^2 \right]_{(3)} \right. \\ &\quad \left. \left[\theta_2^R \times {}^0 \mathbf{t}_F^2 + \mathbf{d}_2^R \right]_{(3)} \right] \cdot \tilde{\mathbf{p}}_1^F. \end{aligned} \quad (9)$$

and

$$\left[{}^0 H_F^2 \cdot \Delta_F^R \cdot \tilde{\mathbf{p}}_1^F \right]_{(3)} = \left[\left[{}^0 \mathbf{a}_F^2 \right]^T \left[\mathbf{p}_1^F \times {}^0 \mathbf{a}_2^F \right]^T \right] \cdot \mathbf{x}_F^R. \quad (10)$$

Similarly, we can get other two equations for \mathbf{p}_2 and \mathbf{p}_3 . Finally, we have

$$\begin{bmatrix} \begin{bmatrix} 0 & \mathbf{a}_2^F \end{bmatrix}^T \\ \begin{bmatrix} 0 & \mathbf{a}_2^F \end{bmatrix}^T \\ \begin{bmatrix} 0 & \mathbf{a}_3^F \end{bmatrix}^T \end{bmatrix} \begin{bmatrix} \mathbf{p}_1^F \times^0 \mathbf{a}_2^F \\ \mathbf{p}_2^F \times^0 \mathbf{a}_2^F \\ \mathbf{p}_3^F \times^0 \mathbf{a}_3^F \end{bmatrix}^T \cdot \mathbf{x}_F^R = \begin{bmatrix} \begin{bmatrix} \boldsymbol{\theta}_2^R \times^0 \mathbf{n}_F^2 \\ \boldsymbol{\theta}_2^R \times^0 \mathbf{o}_F^2 \end{bmatrix}_{(3)} \begin{bmatrix} \boldsymbol{\theta}_2^R \times^0 \mathbf{a}_F^2 \\ \boldsymbol{\theta}_2^R \times^0 \mathbf{t}_F^2 + \mathbf{d}_2^R \end{bmatrix}_{(3)} \cdot \tilde{\mathbf{p}}_1^F \\ \begin{bmatrix} \boldsymbol{\theta}_2^R \times^0 \mathbf{n}_F^2 \\ \boldsymbol{\theta}_2^R \times^0 \mathbf{o}_F^2 \end{bmatrix}_{(3)} \begin{bmatrix} \boldsymbol{\theta}_2^R \times^0 \mathbf{a}_F^2 \\ \boldsymbol{\theta}_2^R \times^0 \mathbf{t}_F^2 + \mathbf{d}_2^R \end{bmatrix}_{(3)} \cdot \tilde{\mathbf{p}}_2^F \\ \begin{bmatrix} \boldsymbol{\theta}_3^R \times^0 \mathbf{n}_F^3 \\ \boldsymbol{\theta}_3^R \times^0 \mathbf{o}_F^3 \end{bmatrix}_{(3)} \begin{bmatrix} \boldsymbol{\theta}_3^R \times^0 \mathbf{a}_F^3 \\ \boldsymbol{\theta}_3^R \times^0 \mathbf{t}_F^3 + \mathbf{d}_3^R \end{bmatrix}_{(3)} \cdot \tilde{\mathbf{p}}_3^F \end{bmatrix}. \quad (11)$$

Although there are six parameters in \mathbf{x}_F^R , only three of them are unknown nonzero values. By solving the above equation system, we can obtain the differential motion vector \mathbf{x}_F^R and put it in the form of (4) by rearranging the terms. To guarantee the inverse of the matrix exists, the line passing the two datum points on the second datum plane cannot be perpendicular to the primary datum plane. If so, the first and the second rows of the coefficient matrix of \mathbf{x}_F^R in the left-hand side of (11) will be the same.

The expression of T_1 and T_2 for a general 3-2-1 setup is very complicated. However, if datum fixtures 1, 2, and 3 are orthogonal to each other, which is a very common case in practice, T_1 and T_2 can be significantly simplified. Given the nominal positions for features 2 and 3 and locating pins in Fig. 6(a) as

$${}^0H_F^2 = \begin{bmatrix} 0 & 0 & 1 & 0 & t_{Fx}^2 \\ 0 & 1 & 0 & 0 & t_{Fy}^2 \\ -1 & 0 & 0 & 0 & 0 \\ 0 & 0 & 0 & 1 & 0 \end{bmatrix}, \quad {}^0H_F^3 = \begin{bmatrix} 1 & 0 & 0 & 0 & t_{Fx}^3 \\ 0 & 0 & 1 & 0 & t_{Fy}^3 \\ 0 & -1 & 0 & 0 & 0 \\ 0 & 0 & 0 & 1 & 0 \end{bmatrix}$$

$\mathbf{p}_1^F = [0 \ p_{1y}^F \ p_{1z}^F]^T$, $\mathbf{p}_2^F = [0 \ p_{2y}^F \ p_{2z}^F]^T$, and $\mathbf{p}_3^F = [p_{2x}^F \ 0 \ p_{3z}^F]^T$, the solution of (11) can be obtained as (4), where

$$T_1 = \begin{bmatrix} 0 & 0 & -1 & -0 & t_{Fy}^2 & p_{2z}^F + 0 & t_{Fx}^2 + \frac{p_{2y}^F(p_{2z}^F - p_{1z}^F)}{p_{1y}^F - p_{2y}^F} & 0 \\ 0 & 0 & 0 & -p_{3x}^F & \frac{p_{3x}^F(p_{1z}^F - p_{2z}^F)}{p_{1y}^F - p_{2y}^F} & 0 & 0 & 0 \\ 0 & 0 & 0 & 0 & 0 & 0 & 0 & 0 \\ 0 & 0 & 0 & 0 & 0 & 0 & 0 & 0 \\ 0 & 0 & 0 & 0 & 0 & 0 & 0 & 0 \\ 0 & 0 & 0 & 1 & -\frac{p_{1z}^F - p_{2z}^F}{p_{1y}^F - p_{2y}^F} & 0 & 0 & 0 \end{bmatrix}$$

$$T_2 = \begin{bmatrix} 0 & 0 & 0 & 0 & 0 & 0 & 0 & 0 \\ 0 & 0 & -1 & -p_{3z}^F & -0 & t_{Fy}^3 & p_{3x}^F + 0 & t_{Fx}^3 \\ 0 & 0 & 0 & 0 & 0 & 0 & 0 & 0 \\ 0 & 0 & 0 & 0 & 0 & 0 & 0 & 0 \\ 0 & 0 & 0 & 0 & 0 & 0 & 0 & 0 \\ 0 & 0 & 0 & 0 & 0 & 0 & 0 & 0 \end{bmatrix}.$$

A very common variation of the general 3-2-1 fixture setup is shown in Fig. 6(b). The six degree of freedoms of the workpiece are constrained by the plane ABCD (two rotational and one translational motion), a circular short hole P_1 and P_3 (two translational motion), and a slot P_2 (one rotational motion). Given the nominal positions for features 2 and 3 and locating pins in Fig. 6(b) as

$${}^0H_F^2 = \begin{bmatrix} 0 & 0 & 1 & 0 \\ 0 & 1 & 0 & 0 \\ -1 & 0 & 0 & 0 \\ 0 & 0 & 0 & 1 \end{bmatrix}, \quad {}^0H_F^3 = \begin{bmatrix} 1 & 0 & 0 & 0 \\ 0 & 0 & 1 & 0 \\ 0 & -1 & 0 & 0 \\ 0 & 0 & 0 & 1 \end{bmatrix}$$

$\mathbf{p}_1^F = [0 \ 0 \ 0]^T$, $\mathbf{p}_2^F = [0 \ p_{2y}^F \ 0]^T$ and $\mathbf{p}_3^F = [0 \ 0 \ 0]^T$, the solution of (11) can be obtained as (4), where

$$T_1 = \begin{bmatrix} 0 & 0 & -1 & 0 & 0 & 0 \\ 0 & 0 & 0 & 0 & 0 & 0 \\ 0 & 0 & 0 & 0 & 0 & 0 \\ 0 & 0 & 0 & 0 & 0 & 0 \\ 0 & 0 & 0 & 0 & 0 & 0 \\ 0 & 0 & 0 & 1 & 0 & 0 \end{bmatrix} \text{ and } T_2 = \begin{bmatrix} 0 & 0 & 0 & 0 & 0 & 0 \\ 0 & 0 & -1 & 0 & 0 & 0 \\ 0 & 0 & 0 & 0 & 0 & 0 \\ 0 & 0 & 0 & 0 & 0 & 0 \\ 0 & 0 & 0 & 0 & 0 & 0 \\ 0 & 0 & 0 & 0 & 0 & 0 \end{bmatrix}.$$

The procedure presented in this section can be used to study the datum-induced error for a general 3-2-1 fixture setup. Following the same deviation, similar results can be obtained for other fixture setups, such as that used in turning operations.

2) *Analysis of Fixture Errors*: In a general 3-2-1 fixture scheme as shown in Fig. 6(a), the workpiece position is located by six locators ($P_1, P_2, P_3, L_1, L_2, L_3$). Assume that the nominal coordinates of these six points in the nominal fixture coordinate system 0FCS are $(0, p_{1y}, p_{1z})$, $(0, p_{2y}, p_{2z})$, $(p_{3x}, 0, p_{3z})$, $(L_{1x}, L_{1y}, 0)$, $(L_{2x}, L_{2y}, 0)$, and $(L_{3x}, L_{3y}, 0)$, respectively. (Note that we assume that the z coordinates of P_1 and P_2 are the same to simplify the problem). If there are small deviations on these six locators $(\Delta p_{ix}, \Delta p_{iy}, \Delta p_{iz})$ and $(\Delta L_{ix}, \Delta L_{iy}, \Delta L_{iz})$, where $i = 1, 2, 3$, the actual fixture coordinate system FCS will deviate from its nominal 0FCS . Cai *et al.* [15] gave an analytical infinitesimal error analysis for a rigid body locating scheme with general six points. The fixture error can be derived based on their results. In Fig. 6, the surface norm vector for L_1, L_2 , and L_3 is $(0, 0, 1)$, for P_1 and P_2 is $(-1, 0, 0)$, and for P_3 is $(0, -1, 0)$. With the locators' position vectors, [15, eq. (3.1.6)] can be applied to obtain the deviation of FCS w.r.t. 0FCS as $\mathbf{x}_{FCS}^{0FCS} = T_3[\Delta L_{1z} \ \Delta L_{2z} \ \Delta L_{3z} \ \Delta P_{1x} \ \Delta P_{2x} \ \Delta P_{3y}]^T$, where we have the equation shown at the bottom of the next page, and $C = L_{3x}L_{1y} - L_{1y}L_{2x} + L_{3y}L_{2x} + L_{2y}L_{1x} - L_{2y}L_{3x} - L_{3y}L_{1x}$.

We need to know \mathbf{x}_{FCS}^{0FCS} as well. Note that ${}^0H_{FCS}^{0FCS}$ is an identity matrix, $H_{FCS}^{0FCS} = ({}^0H_{FCS}^{0FCS}) \cdot (\delta H_{FCS}^{0FCS}) = (\delta H_{FCS}^{0FCS})$. On the other hand, $H_{FCS}^{0FCS} = (H_{FCS}^{0FCS})^{-1} = (\delta H_{FCS}^{0FCS})^{-1} \cdot ({}^0H_{FCS}^{0FCS})^{-1} = (\delta H_{FCS}^{0FCS})^{-1}$. It is clear that $(\delta H_{FCS}^{0FCS}) = (\delta H_{FCS}^{0FCS})^{-1}$. From (A8), we have

$$\mathbf{x}_{FCS}^{0FCS} = -\mathbf{x}_{FCS}^{0FCS} = -T_3 \times [\Delta L_{1z} \ \Delta L_{2z} \ \Delta L_{3z} \ \Delta P_{1x} \ \Delta P_{2x} \ \Delta P_{3y}]^T. \quad (12)$$

For the fixture setup shown in Fig. 6(b), the nominal coordinates of P_1, P_2 , and P_3 in 0FCS are $(0, 0, 0)$, $(0, p_{2y}, 0)$, and $(0, 0, 0)$, respectively. Substituting these values into the expression of T_3 , we can obtain another T_3 matrix for the particular setup shown in Fig. 6(b) as

$$T_3 = \begin{bmatrix} 0 & 0 & 0 & 1 & 0 & 0 \\ 0 & 0 & 0 & 0 & 0 & 1 \\ \frac{(L_{3y}L_{2x} - L_{2y}L_{3x})}{c} & \frac{(L_{3x}L_{1y} - L_{3y}L_{1x})}{c} & \frac{(L_{2y}L_{1x} - L_{1y}L_{2x})}{c} & 0 & 0 & 0 \\ \frac{(L_{2x} - L_{3x})}{c} & \frac{(L_{3x} - L_{1x})}{c} & \frac{(L_{1x} - L_{2x})}{c} & 0 & 0 & 0 \\ \frac{(L_{2y} - L_{3y})}{c} & \frac{(L_{3y} - L_{1y})}{c} & \frac{(L_{1y} - L_{2y})}{c} & 0 & 0 & 0 \\ 0 & 0 & 0 & \frac{-1}{p_{2y}} & \frac{1}{p_{2y}} & 0 \end{bmatrix}.$$

The fixture error analysis procedure for a general 3-2-1 fixture scheme is presented in this section. For other fixture systems, the analysis can follow a very similar procedure.

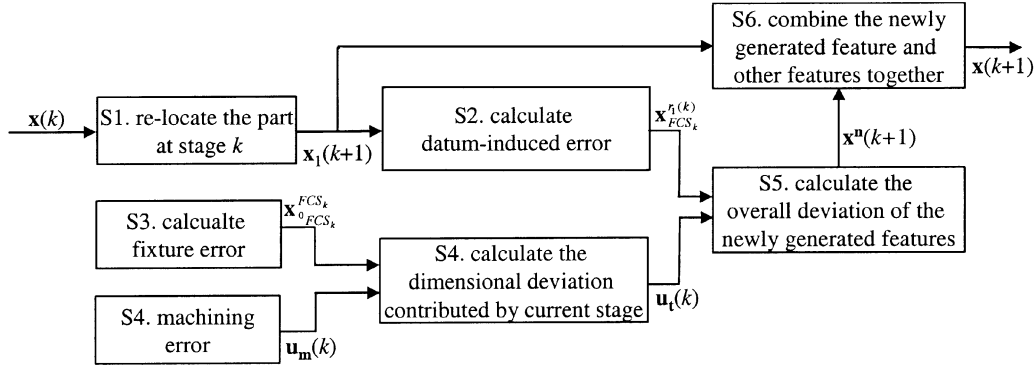


Fig. 7. Steps of the derivation of variation propagation model.

3) *Procedures for Variation Propagation Modeling*: Fig. 7 shows the steps of the derivation of the variation propagation model. The first step is to re-locate the workpiece at current stage k . The second step calculates the datum-induced error, which is caused by dimensional errors generated in previous stages. The third and fourth steps calculate the contribution of fixture error and machining error that are only related with current stage. The fifth stage combines all errors together to obtain the deviation of the newly generated features. Finally, at the sixth step, the newly generated features are combined with other features to form $\mathbf{x}(k+1)$. The detailed derivations are as follows.

S1. Using Corollary 2, transform $\mathbf{x}(k)$ from a stack of $\mathbf{x}_i^{r_1(k-1)}$ to a stack of $\mathbf{x}_i^{r_1(k)}$, ($i = 1, \dots, M$). $r_1(k)$ is the feature index of the primary datum of stage k . Let $\mathbf{x}_1(k+1)$ be the stack of $\mathbf{x}_i^{r_1(k)}$, then

$$\mathbf{x}_1(k+1) = A_1(k)\mathbf{x}(k) \quad (13)$$

where

$$\mathbf{x}_1(k+1) = \begin{bmatrix} \mathbf{x}_1^{r_1(k)} \\ \vdots \\ \mathbf{x}_{s_i(k)}^{r_1(k)} \\ \vdots \\ \mathbf{x}_{r_1(k)}^{r_1(k)} \\ \vdots \\ \mathbf{x}_M^{r_1(k)} \end{bmatrix}$$

$$A_1(k) = \begin{bmatrix} I_{6 \times 6} & \cdots & \mathbf{0} & \cdots & \mathbf{0} & \cdots & \mathbf{0} \\ \vdots & \vdots & \vdots & \vdots & \vdots & \vdots & \vdots \\ \mathbf{0} & \cdots & I_{6 \times 6} & \cdots & Q_{s_i(k)}^{r_1(k)} & \cdots & \mathbf{0} \\ \vdots & \vdots & \vdots & \vdots & \vdots & \vdots & \vdots \\ \mathbf{0} & \cdots & \mathbf{0} & \cdots & \mathbf{0} & \cdots & \mathbf{0} \\ \vdots & \vdots & \vdots & \vdots & \vdots & \vdots & \vdots \\ \mathbf{0} & \cdots & \mathbf{0} & \cdots & \mathbf{0} & \cdots & I_{6 \times 6} \end{bmatrix}$$

$$\mathbf{x}(k) = \begin{bmatrix} \mathbf{x}_1^{r_1(k-1)} \\ \vdots \\ \mathbf{x}_{s_i(k)}^{r_1(k-1)} \\ \vdots \\ \mathbf{x}_{r_1(k)}^{r_1(k-1)} \\ \vdots \\ \mathbf{x}_M^{r_1(k-1)} \end{bmatrix}$$

$$Q_{s_i(k)}^{r_1(k)} = \begin{bmatrix} -\left({}^0R_{s_i(k)}^{r_1(k)}\right)^T & \left({}^0R_{s_i(k)}^{r_1(k)}\right)^T \cdot \left({}^0\hat{\mathbf{t}}_{s_i(k)}^{r_1(k)}\right) \\ \mathbf{0} & -\left({}^0R_{s_i(k)}^{r_1(k)}\right)^T \end{bmatrix}$$

where i is an integer from 1 to the total number of features generated up to stage k . In (13), $\mathbf{x}_1(k+1) \in \mathfrak{R}^{6M \times 1}$, $A_1(k) \in \mathfrak{R}^{6M \times 6M}$. If primary datum is not changed between stage $k-1$ and stage k , $\mathbf{x}_1(k+1)$ equals $\mathbf{x}(k)$.

S2. Following the procedure of datum-induced error analysis in Section III, find datum error $\mathbf{x}_{FCS_k}^{r_1(k)}$ as

$$\mathbf{x}_{FCS_k}^{r_1(k)} = A_2(k)\mathbf{x}_1(k+1) \quad (14)$$

$$T_3 = \begin{bmatrix} \frac{(L_{2y} - L_{3y})p_{1z}}{c} & \frac{(L_{3y} - L_{1y})p_{1z}}{c} & \frac{(L_{3y} - L_{2y})p_{1z}}{c} & \frac{-p_{2y}}{(p_{1y} - p_{2y})} & \frac{p_{1y}}{(p_{1y} - p_{2y})} & 0 \\ \frac{(L_{3x} - L_{2x})p_{3z}}{c} & \frac{(L_{1x} - L_{3x})p_{3z}}{c} & \frac{(L_{2x} - L_{1x})p_{3z}}{c} & \frac{p_{3x}}{(p_{1y} - p_{2y})} & \frac{-p_{3x}}{(p_{1y} - p_{2y})} & 1 \\ \frac{(L_{3y}L_{2x} - L_{2y}L_{3x})}{c} & \frac{(L_{3x}L_{1y} - L_{3y}L_{1x})}{c} & \frac{(L_{2y}L_{1x} - L_{1y}L_{2x})}{c} & 0 & 0 & 0 \\ \frac{(L_{2x} - L_{3x})}{c} & \frac{(L_{3x} - L_{1x})}{c} & \frac{(L_{1x} - L_{2x})}{c} & 0 & 0 & 0 \\ \frac{(L_{2y} - L_{3y})}{c} & \frac{(L_{3y} - L_{1y})}{c} & \frac{(L_{1y} - L_{2y})}{c} & 0 & 0 & 0 \\ 0 & 0 & 0 & \frac{1}{(p_{1y} - p_{2y})} & \frac{-1}{(p_{1y} - p_{2y})} & 0 \end{bmatrix}$$

where $A_2(k) = [\mathbf{0} \dots T_1(k) \dots T_2(k) \dots \mathbf{0}]$. The dimension of $A_2(k)$ is 6 by $6M$.

S3. Denoting the fixture imperfection as $\mathbf{u}_f(k)$, we can obtain the fixture error following the procedure of fixture error analysis in Section III, $\mathbf{x}_{0_{FCS_k}^{FCS_k}}$, as

$$\mathbf{x}_{0_{FCS_k}^{FCS_k}} = A_3(k)\mathbf{u}_f(k) \quad (15)$$

where $A_3(k) = -T_3(k)$.

S4. Because the machine tool is calibrated based on ${}^0\text{FCS}$, the tool path imperfection is often represented as a deviation w.r.t. ${}^0\text{FCS}$. Denoting the machining error of newly generated feature $q_i(k)$, i is from 1 to $l(k)$, as $\mathbf{x}_{q_i(k)}^{0_{FCS_k}^{FCS_k}}$ and stack them up as $\mathbf{u}_m(k)$. Using Corollary 1, we can find $\mathbf{x}_{q_i(k)}^{FCS_k}$. Denote $\mathbf{u}_t(k)$ as a stack up of $\mathbf{x}_{q_i(k)}^{FCS_k}$, $i = 1 \dots l(k)$, yields

$$\mathbf{u}_t(k) = A_4(k)\mathbf{x}_{0_{FCS_k}^{FCS_k}} + \mathbf{u}_m(k) \quad (16)$$

where $A_4(k) = [G_{q_1(k)}^T \dots G_{q_i(k)}^T \dots G_{q_{l(k)}(k)}^T]^T$ and $G_{q_i(k)} = \begin{bmatrix} \left({}^0R_{q_i(k)}^{0_{FCS_k}^{FCS_k}} \right)^T & - \left({}^0R_{q_i(k)}^{0_{FCS_k}^{FCS_k}} \right)^T \cdot \left({}^0\hat{\mathbf{t}}_{q_i(k)}^{0_{FCS_k}^{FCS_k}} \right) \\ \mathbf{0} & \left({}^0R_{q_i(k)}^{0_{FCS_k}^{FCS_k}} \right)^T \end{bmatrix}$.

In (16), $\mathbf{u}_t(k) \in \mathbb{R}^{6l(k) \times 1}$, $A_4(k) \in \mathbb{R}^{6l(k) \times 6}$, $\mathbf{x}_{0_{FCS_k}^{FCS_k}} \in \mathbb{R}^{6 \times 1}$ and $\mathbf{u}_m(k) \in \mathbb{R}^{6l(k) \times 1}$.

S5. Based on $\mathbf{x}_{FCS_k}^{r_1(k)}$ from step 2 and $\mathbf{x}_{q_i(k)}^{FCS_k}$ from step 4, we can use Corollary 1 again to obtain the deviations of the newly generated features with respect to RCS, $\mathbf{x}_{q_i(k)}^{r_1(k)}$, $i = 1 \dots l(k)$.

In more detail, denoting $\mathbf{x}^n(k+1)$ as a stack of $\mathbf{X}_{q_i(k)}^{r_1(k)}$ yields

$$\mathbf{x}^n(k+1) = A_4(k) \cdot \mathbf{x}_{FCS_k}^{r_1(k)} + \mathbf{u}_t(k). \quad (17)$$

Note that in (17) an approximation

$$\begin{bmatrix} \left({}^0R_{q_i(k)}^{0_{FCS_k}^{FCS_k}} \right)^T & - \left({}^0R_{q_i(k)}^{0_{FCS_k}^{FCS_k}} \right)^T \cdot \left({}^0\hat{\mathbf{t}}_{q_i(k)}^{0_{FCS_k}^{FCS_k}} \right) \\ \mathbf{0} & \left({}^0R_{q_i(k)}^{0_{FCS_k}^{FCS_k}} \right)^T \end{bmatrix} \mathbf{x}_{FCS_k}^{r_1(k)} \approx \begin{bmatrix} \left({}^0R_{q_i(k)}^{FCS_k} \right)^T & - \left({}^0R_{q_i(k)}^{FCS_k} \right)^T \cdot \left({}^0\hat{\mathbf{t}}_{q_i(k)}^{FCS_k} \right) \\ \mathbf{0} & \left({}^0R_{q_i(k)}^{FCS_k} \right)^T \end{bmatrix} \mathbf{x}_{FCS_k}^{r_1(k)} \quad (18)$$

is used because $\Delta_{0_{FCS_k}^{FCS_k}}$ and $\mathbf{x}_{FCS_k}^{r_1(k)}$ are both small values. The details are as follows. First note that ${}^0H_{q_i(k)}^{FCS_k} = H_{0_{FCS_k}^{FCS_k}}^{FCS_k}$. ${}^0H_{q_i(k)}^{0_{FCS_k}^{FCS_k}} = {}^0H_{0_{FCS_k}^{FCS_k}}^{FCS_k} \cdot (I + \Delta_{0_{FCS_k}^{FCS_k}}) \cdot {}^0H_{q_i(k)}^{0_{FCS_k}^{FCS_k}}$. Since ${}^0H_{0_{FCS_k}^{FCS_k}}^{FCS_k} = I_{4 \times 4}$, ${}^0H_{q_i(k)}^{FCS_k} = {}^0H_{q_i(k)}^{0_{FCS_k}^{FCS_k}} + \Delta_{0_{FCS_k}^{FCS_k}} \cdot {}^0H_{q_i(k)}^{0_{FCS_k}^{FCS_k}}$, or see (19), shown at the bottom of the page. Hence

$$\begin{aligned} {}^0R_{q_i(k)}^{FCS_k} &= {}^0R_{q_i(k)}^{0_{FCS_k}^{FCS_k}} + \hat{\theta}_{0_{FCS_k}^{FCS_k}}^{FCS_k} \cdot {}^0R_{q_i(k)}^{0_{FCS_k}^{FCS_k}} \\ {}^0\hat{\mathbf{t}}_{q_i(k)}^{FCS_k} &= {}^0\hat{\mathbf{t}}_{q_i(k)}^{0_{FCS_k}^{FCS_k}} + \hat{\theta}_{0_{FCS_k}^{FCS_k}}^{FCS_k} \cdot {}^0\hat{\mathbf{t}}_{q_i(k)}^{0_{FCS_k}^{FCS_k}} + \mathbf{d}_{0_{FCS_k}^{FCS_k}}^{FCS_k}. \end{aligned} \quad (20)$$

Substituting (20) into the right-hand side of (18) and neglecting the second-order small values yields the approximation result of (18).

S6. Adding the newly generated features with the others yields $\mathbf{x}(k+1)$ as follows:

$$\mathbf{x}(k+1) = \mathbf{x}_1(k+1) + A_5(k)\mathbf{x}^n(k+1) \quad (21)$$

where $A_5(k)$ is a selector matrix in the form

$$A_5(k) = \begin{bmatrix} \mathbf{0} & \dots & \mathbf{0} & \dots & \mathbf{0} \\ \vdots & \vdots & \vdots & \vdots & \vdots \\ I_{6 \times 6} & \dots & \dots & \dots & \dots \\ \vdots & \vdots & \vdots & \vdots & \vdots \\ \mathbf{0} & \dots & I_{6 \times 6} & \dots & \mathbf{0} \\ \vdots & \vdots & \vdots & \vdots & \vdots \\ \mathbf{0} & \dots & \mathbf{0} & \dots & I_{6 \times 6} \\ \vdots & \vdots & \vdots & \vdots & \vdots \\ \mathbf{0} & \dots & \mathbf{0} & \dots & \mathbf{0} \end{bmatrix}.$$

Its dimension is $6M$ by $6 \times l(k)$ and it places the deviations of the newly generated features on the corresponding location when they are added to $\mathbf{x}_1(k+1)$.

Considering (13)–(21), we can get the state transition equation for the state space model

$$\begin{aligned} \mathbf{x}(k+1) &= [A_1(k) + A_5(k)A_4(k)A_2(k)A_1(k)]\mathbf{x}(k) \\ &+ [A_5(k)A_4(k)A_3(k)A_5(k) \begin{bmatrix} \mathbf{x}_f(k) \\ \mathbf{u}_m(k) \end{bmatrix}]. \end{aligned} \quad (22)$$

The detailed derivation can be found in Appendix III. In (1), $A(k) = A_1(k) + A_5(k)A_4(k)A_2(k)A_1(k)$, $B(k) = [A_5(k)A_4(k)A_3(k)A_5(k)]$ and $\mathbf{u}(k) = [\mathbf{u}_f(k)^T \mathbf{u}_m(k)^T]^T$.

The derivation of the observation equation in (1) is straightforward. The measurement stage can be viewed as a special machining stage. Assume that feature $r_m(k)$ is used as the measurement reference feature and denote $\mathbf{x}_m(k)$ as the stack of $\mathbf{x}_i^{r_m(k)}$, following the same derivation of Step 1, we can obtain

$$\mathbf{x}_m(k) = A_m(k)\mathbf{x}(k) \quad (23)$$

where $A_m(k)$ has the same format as $A_1(k)$ in (13) except that $r_m(k)$ is used in the place of $r_1(k)$. Hence, the observation equation can be written as

$$\mathbf{y}(k) = C_m(k)A_m(k)\mathbf{x}(k) \quad (24)$$

where $C_m(k)$ is a selector matrix that is similar to the format of $A_5(k)$ in (21). $C_m(k)$ selects the measured features among all the available features. Therefore, in (1), the observation equation is

$$C(k) = C_m(k)A_m(k). \quad (25)$$

The above model describes the deviation propagation among a multistage machining process. An experimental validation of this model is presented in Section IV.

$${}^0H_{q_i(k)}^{FCS_k} = \begin{bmatrix} {}^0R_{q_i(k)}^{0_{FCS_k}^{FCS_k}} + \hat{\theta}_{0_{FCS_k}^{FCS_k}}^{FCS_k} \cdot {}^0R_{q_i(k)}^{0_{FCS_k}^{FCS_k}} & {}^0\hat{\mathbf{t}}_{q_i(k)}^{0_{FCS_k}^{FCS_k}} + \hat{\theta}_{0_{FCS_k}^{FCS_k}}^{FCS_k} \cdot {}^0\hat{\mathbf{t}}_{q_i(k)}^{0_{FCS_k}^{FCS_k}} + \mathbf{d}_{0_{FCS_k}^{FCS_k}}^{FCS_k} \\ \mathbf{0} & 1 \end{bmatrix} \quad (19)$$

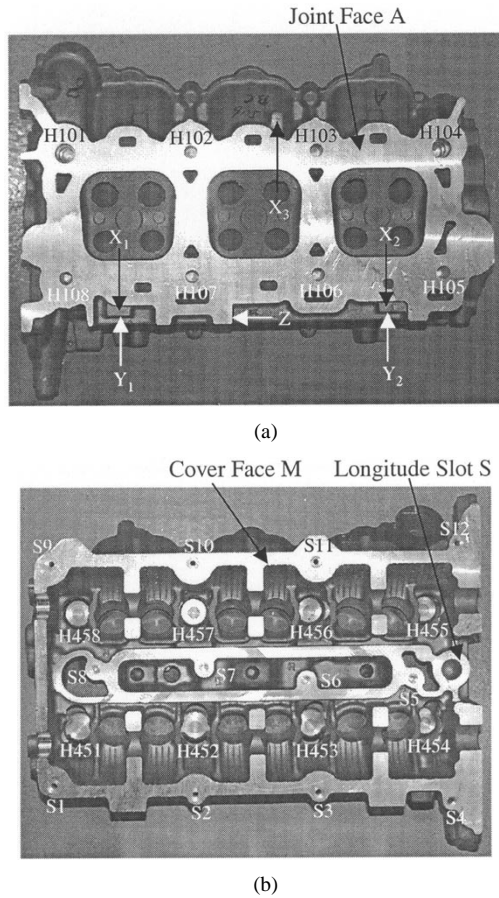


Fig. 8. Final product. (a) Joint face of the engine head. (b) Cover face of the engine head.

IV. EXPERIMENTAL VALIDATION OF THE STATE SPACE VARIATION PROPAGATION MODEL

The deviation propagation model is validated on a multistage machining process developed at the NSF Engineering Research Center for Reconfigurable Machining Systems. The process is introduced as follows.

A. Experimental Machining Process

The product is a V-6 automotive engine head. Its key features are shown in Fig. 8. H101~H108 are eight bolt holes on the joint face. H101 and H104 are also called the locating holes B and C. $X_1, X_2, X_3, Y_1, Y_2, Z$ are the cast rough datum. H451~H458 are eight bolt holes on the cover face. S1~S12 are twelve screw holes on the cover face.

There are three operations in this process. Each operation and corresponding datum setup are shown in Figs. 9 and 10 and Table I.

The major tolerances on these key features are shown in Fig. 11 and Table II. In Fig. 11, surface D is defined by the rough data $X_1, X_2,$ and X_3 .

B. State Space Modeling of the Process

A state space model that contents six features is developed for this case study. Their nominal positions and orientations are listed in Table III. These numbers in Table III are with respect to the part reference coordinate system. The origin of the part

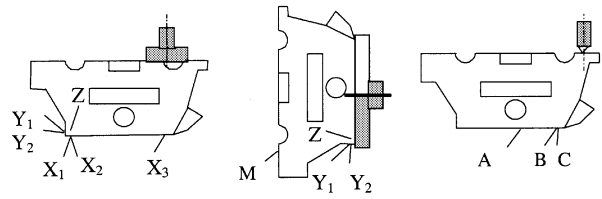


Fig. 9. Operation sequence.

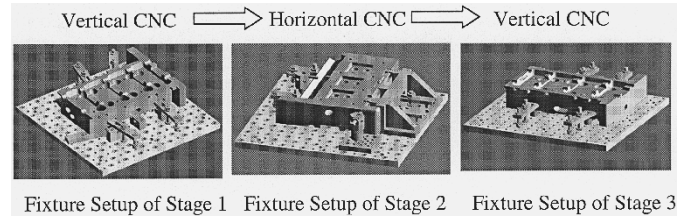


Fig. 10. Fixture locating schemes in three stages.

reference coordinate is the intersection point between the center line of hole B and the plane determined by rough datum $X_1, X_2,$ and X_3 , the y axis is the line connecting the centers of hole B and hole C, the z axis coincides with the centerline of hole B and points from the cover face to the joint face, the x axis is determined by the right-hand principle. From Table III, it is straightforward to obtain the nominal relationship between any two features.

Following the procedure shown in Section III, a state space model can be obtained for this three-stage machining process. The state space model can be obtained as

$$\mathbf{x}(k+1) = \mathbf{A}(k)\mathbf{x}(k) + \mathbf{B}(k)\mathbf{u}(k) + \mathbf{w}(k), \quad k = 1, 2, 3 \quad (26)$$

$$\mathbf{y}(k) = \mathbf{C}(k)\mathbf{x}(k) + \mathbf{v}(k). \quad (27)$$

The details of the system matrices are listed in Appendix IV.

C. Comparison Between the Real Measurement and the Model Prediction

To validate the model, a workpiece is machined in this testbed. In the machining, a fixture error is intentionally added to the process at each stage. The inputs to the model that corresponds to the fixture error are

$$\mathbf{u}_f(1) = [0 \ 0 \ -0.20 \ 0 \ 0 \ 0]$$

$$\mathbf{u}_f(2) = [-0.39 \ 0 \ 0 \ 0 \ 0 \ 0]$$

$$\mathbf{u}_f(3) = [-0.39 \ 0 \ 0 \ 0 \ 0 \ 0].$$

The nonzero values in $\mathbf{u}_f(k)$ correspond to the magnitudes of the fixture errors. All the inputs corresponding to the machining error $\mathbf{u}_m(k)$ are set as zeros. The workpiece is measured on a CMM after machining. The measurement results from CMM are listed in Table IV. For a plane feature, the CMM measurement gives the coordinates of a point on the surface and the norm direction vector of the surface. For the cylinder (Hole B and Hole C) feature, the CMM measurement gives the coordinate of a point on the cylinder axis, the norm direction vector of the axis, and the diameter. The diameters of the holes are not listed in the table because they are not used in this study.

All the measurements are with respect to the global CMM coordinate system. These data can easily be transformed to the

TABLE I
DESCRIPTION OF THE OPERATIONS

Operation #	Locating Datum (Primary +Secondary +Tertiary)	Operation Descriptions
1	$(X_1, X_2, X_3) + (Y_1, Y_2) + Z$	<ul style="list-style-type: none"> • Mill cover face M • Spot drill H451~H458 • Spot face H451~H458
2	$M + (Y_1, Y_2) + Z$	<ul style="list-style-type: none"> • Mill joint face A • Spot drill H101~H108 • Drill, chamfer, counterboring, and reaming hole H101(B) and H104(C) • Drill H102, 103, and H105~H108
3	$A + B + C$	<ul style="list-style-type: none"> • Mill slot S • Drill and chamfer twelve screw holes S1~S12.

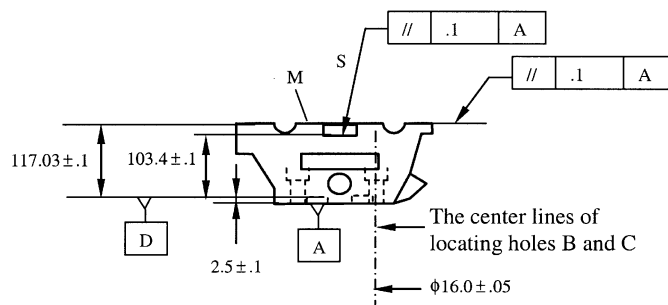


Fig. 11. Major design specifications on the engine head.

same coordinate system used in the state space model. In the state space model, the coefficient matrices A , B , and C and the input to the model u are known. If we neglect the model noise and measurement noise and set the initial state vector $x(1)$ as zero, we can iteratively calculate the state vectors at all the stages by (1). In this way, the measurement value can be predicted. The comparison between the real measurement and the model prediction is listed in Table V. For a plane feature, the relevant parameter is its orientation and the distance from datum plane. The deviation of the orientation of a plane is denoted by $[\theta_1, \theta_2, \theta_3]$ and the deviation of the distance from the datum plane is denoted by d_z . d_z is measured at the origin of LCS of the plane with respect to the datum plane. For the cylinder feature (Hole B and Hole C), only the deviation in orientation is considered.

Remarks:

- From the data presented in Table V, the discrepancies between the model predication and real measurement of joint face, Hole B, and the slot are reasonably small. Since only the dominant fixture errors are taken as the inputs to the model in this case study, these discrepancies are due to other machining errors such as machine geometric error, thermal error, force induced error that are neglected in the input to the model. The small discrepancies between the model prediction and real measurement of these three features show that this model captures the dominant fixture errors correctly.
- Relatively large discrepancies happen at the cover face and Hole C. The large difference at the cover face is understand-

able because the reference datum feature is the rough datum that contains large natural variation itself. The large difference at Hole C is an indication of large geometric error with the machine. Since the joint face, Hole B, and Hole C are machined at the same time under the same setup, they should have the same orientation as the model predicts if only fixture error presents. A difference in the orientation between Hole C, Hole B, and the joint face indicates that the cutting tool orientation is different at different machine configuration, which is considered as a geometric error.

- Another point need to be pointed out is that the deviation patterns (i.e., the sign of each deviation and their relative magnitude) are correctly predicted by the model. This is important because we can conduct root cause identification by considering the error patterns in the measurement.

V. CONCLUSION

The complexity of a multistage machining process places great difficulty on the root cause identification and process design evaluation. In this paper, an analytical linear model is developed to describe the propagation of workpiece geometric deviation among multiple machining stages. This model has a state space form. Using the state transitions among multiple machining stages, this model describes the geometric error accumulation and transformation when the workpiece passes the whole process. A systematic procedure is presented to model the workpiece setup and machining cutting process.

This model has great potential to be applied in the following fields. First, it can be used in the root cause identification for the quality improvement purpose. For a complicated machining process, it is often very difficult, if not impossible, to identify the faulty stage if certain feature of the workpiece is out of specification. With this model that integrates the process and product information, model based fault diagnosis can be developed to quickly identify the faults. Second, based on the diagnosis study, this model can also be used to conduct the sensor placement optimization. How to place sensors in a complicated manufacturing line to minimize the cost and maximize the amount of information obtained is a challenging issue. In this model, the sensor placement information is integrated in the ob-

TABLE II
DESCRIPTION OF TOLERANCE REQUIREMENT

Characteristics	Specifications(mm)	Operation
1. Distance between M and rough datum surface D	117.03 ± 0.1	1 st
2. Distance between A and rough datum surface D	2.5 ± 0.1	2 nd
3. Parallelism between M and A	0.1	
4. Distance between slot S and A	103.4 ± 0.1	3 rd
5. Parallelism between A and S	0.1	

TABLE III
NOMINAL POSITIONS AND ORIENTATIONS OF KEY FEATURES

Feature #	Feature Name	${}^0\omega_i^R$	${}^0\mathbf{t}_i^R$
1	Surface D	[0, 0, 0]	[133.7, 134.2, 0]
2	Joint face A	[0, 0, 0]	[0, 0, 2.5]
3	Cover face M	[0, π , 0]	[0, 0, -117.03]
4	Hole B	[0, 0, 0]	[0, 0, 2.5]
5	Hole C	[0, 0, 0]	[0, 306, 2.5]
6	Slot	[0, π , 0]	[0, 0, -100.9]

TABLE IV
CMM MEASUREMENT RESULTS

	x	y	z	i	j	k
Rough Datum	-361.661	75.708	27.553	-1	-0.005	-0.003
Joint Face	-364.264	103.454	35.086	-1	-0.005	-0.005
Hole B	-357.147	154.084	-132.65	1	0.005	0.005
Hole C	-358.721	153.795	173.319	1	0.003	0.005
Cover Face	-244.887	103.429	45.558	1	0.006	0.003
Slot	-261.027	99.433	31.59	1	0.008	0.005

TABLE V
COMPARISON BETWEEN THE MEASUREMENT AND THE MODEL PREDICTION

	Measurement				Model Output			
	θ_1	θ_2	θ_3	d_z	θ_1	θ_2	θ_3	d_z
Cover Face w.r.t. Rough Datum	0.0000	0.0010	0.0000	-0.113	0.0000	0.0012	0	-0.157
Joint Face w.r.t. Cover Face	0.0020	-0.0010	0.0000	-0.508	0.0019	-0.0012	0	-0.483
Hole B w.r.t. Cover Face	0.0020	-0.0010	0.0000	-	0.0019	-0.0012	0	-
Hole C w.r.t. Cover Face	0.0020	-0.0030	0.0000	-	0.0019	-0.0012	0	-
Slot w.r.t. Joint Face	0.0000	0.0030	0.0000	-0.370	0	0.0037	0	-0.353

servation matrix $C(k)$. Using this analytical state space model, one can apply some classical concepts from control theory, such as the ‘‘observability,’’ to study the sensor placement problem. Third, this model can also be used for variation simulation of multistage machining process. Using the developed analytical state space model, the variation simulation can be conducted with given initial conditions. This kind of simulation is valuable for process design evaluation. Using the simulation result, we can make selection among several design alternatives regarding their robustness to variation propagation. Fourth, this model can be used for fixture design and optimization. This model provides

a quantitative relationship between the fixture locator errors and the final workpiece geometric error. By considering this relationship, the fixture locator design can be evaluated and optimized. All these potential works will be pursued and reported in the future.

APPENDIX I

Given the location vector and the roll, pitch, and yaw angles, LCS_n can be expressed in RCS by a 4×4 HTM H_n^R . The right superscript R refers to RCS and the right subscript n refers to

the index of LCS. ${}^0H_n^R$ represents the nominal HTM between the RCS and the LCS. A HTM can be written as

$$H_n^R = \begin{bmatrix} R_n^R & \mathbf{t}_n^R \\ \mathbf{0} & 1 \end{bmatrix}.$$

\mathbf{t}_n^R is the location vector of the origin of LCS_n expressed in RCS and R_n^R is the rotational matrix. Some useful properties of HTM are listed as follows (see [9] and [16]).

- A point expressed in LCS_n can be transformed into RCS, i.e., $\mathbf{p}^R = H_n^R \mathbf{p}^n$, where the superscript shows in which coordinate system the point is expressed.
- A rotational matrix is a special orthogonal matrix. $R^{-1} = R^T$ and $\det(R) = 1$.
- $H_R^n = (H_n^R)^{-1}$ and it can be obtained as
$$H_R^n = \begin{bmatrix} (R_n^R)^T & -(R_n^R)^T \mathbf{t}_n^R \\ \mathbf{0} & 1 \end{bmatrix}.$$

A small deviation of LCS_n from its nominal position and orientation can be described by a differential motion vector

$$\mathbf{x}_n^R = \begin{bmatrix} \mathbf{d}_n^R \\ \boldsymbol{\theta}_n^R \end{bmatrix} \quad (\text{A1})$$

where $\mathbf{d}_n^R = [d_{nx}^R \ d_{ny}^R \ d_{nz}^R]^T$ and $\boldsymbol{\theta}_n^R = [\theta_{nx}^R \ \theta_{ny}^R \ \theta_{nz}^R]^T$ are a small position deviation and a small orientation deviation, respectively. If we define

$$\begin{aligned} \text{Trans}(d_x, d_y, d_z) &= \begin{bmatrix} 1 & 0 & 0 & d_x \\ 0 & 1 & 0 & d_y \\ 0 & 0 & 1 & d_z \\ 0 & 0 & 0 & 1 \end{bmatrix} \\ \text{Rot}(x, \theta) &= \begin{bmatrix} 1 & 0 & 0 & 0 \\ 0 & 1 & -\theta & 0 \\ 0 & \theta & 1 & 0 \\ 0 & 0 & 0 & 1 \end{bmatrix} \\ \text{Rot}(y, \theta) &= \begin{bmatrix} 1 & 0 & \theta & 0 \\ 0 & 1 & 0 & 0 \\ -\theta & 0 & 1 & 0 \\ 0 & 0 & 0 & 1 \end{bmatrix} \quad \text{and} \\ \text{Rot}(z, \theta) &= \begin{bmatrix} 1 & -\theta & 0 & 0 \\ \theta & 1 & 0 & 0 \\ 0 & 0 & 1 & 0 \\ 0 & 0 & 0 & 1 \end{bmatrix} \end{aligned}$$

then the actual HTM and the nominal HTM between the reference and local coordinate systems can be related by

$$H_n^R = {}^0H_n^R \cdot \text{Trans}(d_{nx}^R, d_{ny}^R, d_{nz}^R) \cdot \text{Rot}(x, \theta_{nx}^R) \cdot \text{Rot}(y, \theta_{ny}^R) \cdot \text{Rot}(z, \theta_{nz}^R). \quad (\text{A2})$$

$\text{Trans}(d_{nx}^R, d_{ny}^R, d_{nz}^R) \cdot \text{Rot}(x, \theta_{nx}^R) \cdot \text{Rot}(y, \theta_{ny}^R) \cdot \text{Rot}(z, \theta_{nz}^R)$ is defined as δH_n^R . Hence,

$$H_n^R = {}^0H_n^R \cdot \delta H_n^R. \quad (\text{A3})$$

δH_n^R can be written as

$$\delta H_n^R = \begin{bmatrix} 1 & -\theta_{nz}^R & \theta_{ny}^R & d_{nx}^R \\ \theta_{nz}^R & 1 & -\theta_{nx}^R & d_{ny}^R \\ -\theta_{ny}^R & \theta_{nx}^R & 1 & d_{nz}^R \\ 0 & 0 & 0 & 1 \end{bmatrix} = I_{4 \times 4} + \Delta_n^R \quad (\text{A4})$$

where Δ_n^R is called differential transformation matrix (DTM). If a skew symmetric matrix associated with a vector \mathbf{p} is defined

$$\text{as } \hat{\mathbf{p}} = \begin{bmatrix} 0 & -p_3 & p_2 \\ p_3 & 0 & -p_1 \\ -p_2 & p_1 & 0 \end{bmatrix}, \text{ the DTM can be written as}$$

$$\Delta_n^R = \begin{bmatrix} 0 & -\theta_{nz}^R & \theta_{ny}^R & d_{nx}^R \\ \theta_{nz}^R & 0 & -\theta_{nx}^R & d_{ny}^R \\ -\theta_{ny}^R & \theta_{nx}^R & 0 & d_{nz}^R \\ 0 & 0 & 0 & 0 \end{bmatrix} = \begin{bmatrix} \hat{\boldsymbol{\theta}}_n^R & \mathbf{d}_n^R \\ \mathbf{0} & 0 \end{bmatrix}. \quad (\text{A5})$$

We have

$$H_n^R = {}^0H_n^R + {}^0H_n^R \Delta_n^R. \quad (\text{A6})$$

One very useful fact can be obtained if we use small motion assumption, i.e.,

$$(\delta H_n^R)^{-1} \approx \text{Trans}(-d_{nx}^R, -d_{ny}^R, -d_{nz}^R) \cdot \text{Rot}(x, -\theta_{nx}^R) \cdot \text{Rot}(y, -\theta_{ny}^R) \cdot \text{Rot}(z, -\theta_{nz}^R). \quad (\text{A7})$$

If we let $(\delta H_n^R)^{-1} = I_{4 \times 4} + \bar{\Delta}_n^R$ and $\delta H_n^R = I_{4 \times 4} + \Delta_n^R$, then

$$\bar{\Delta}_n^R = -\Delta_n^R. \quad (\text{A8})$$

APPENDIX II

Proof of Corollary 1: Notice $H_1^R = {}^0H_1^R + {}^0H_1^R \cdot \Delta_1^R$ and $H_2^R = {}^0H_2^R + {}^0H_2^R \cdot \Delta_2^R$, we have $H_2^R = H_1^R H_2^R = {}^0H_2^R + {}^0H_1^R \cdot \Delta_1^R \cdot {}^0H_2^R + {}^0H_2^R \cdot \Delta_2^R + {}^0H_1^R \cdot \Delta_1^R \cdot {}^0H_2^R \cdot \Delta_2^R$. Since the deviations are small, we can neglect the second-order small values, $H_2^R \approx {}^0H_2^R + {}^0H_1^R \cdot \Delta_1^R \cdot {}^0H_2^R + {}^0H_2^R \Delta_2^R = {}^0H_2^R (I + ({}^0H_2^R)^{-1} \cdot \Delta_1^R \cdot {}^0H_2^R + \Delta_2^R)$. Noting that $H_2^R = {}^0H_2^R (I + \Delta_2^R)$, we have

$$\Delta_2^R = ({}^0H_2^R)^{-1} \cdot \Delta_1^R \cdot {}^0H_2^R + \Delta_2^R. \quad (\text{A9})$$

Denoting the differential motion vector associated with Δ_1^R as \mathbf{x}_1^R , then the differential motion vector associated with $({}^0H_2^R)^{-1} \cdot \Delta_1^R \cdot {}^0H_2^R$ is

$$\begin{bmatrix} ({}^0R_2^R)^T & -({}^0R_2^R)^T \cdot ({}^0\hat{\mathbf{t}}_2^R) \\ \mathbf{0} & ({}^0R_2^R)^T \end{bmatrix} \mathbf{x}_1^R$$

as in [9]. Combining this result with (A9), yields (2).

Proof of Corollary 2: Noting $H_1^R = {}^0H_1^R \cdot \delta H_1^R$, we have $H_R^R = (\delta H_1^R)^{-1} \cdot {}^0H_1^R$. Then, $H_2^R = H_R^R H_2^R = (\delta H_1^R)^{-1} \cdot {}^0H_1^R \cdot {}^0H_2^R \cdot \delta H_2^R$. Considering (A4) and (A8) yields

$$H_2^R = {}^0H_2^R \cdot ({}^0H_2^R)^{-1} \cdot (-\Delta_1^R + I) \cdot {}^0H_2^R \cdot (\Delta_2^R + I). \quad (\text{A10})$$

Therefore,

$$\delta H_2^R = ({}^0H_2^R)^{-1} \cdot (-\Delta_1^R + I) \cdot {}^0H_2^R \cdot (\Delta_2^R + I). \quad (\text{A11})$$

This equation can be further simplified by neglecting the second-order small values

$$\delta H_2^R \approx ({}^0H_2^R)^{-1} \cdot (-\Delta_1^R) \cdot {}^0H_2^R + ({}^0H_2^R)^{-1} \cdot {}^0H_2^R \cdot \Delta_2^R + I. \quad (\text{A12})$$

$$\Delta_2^R = ({}^0H_2^R)^{-1} \cdot (-\Delta_1^R) \cdot {}^0H_2^R + \Delta_2^R. \quad (\text{A13})$$

By (A13) and using the result from [9] again, we can get the result in (3).

In the model for experimental validation, the measurement starts from $x(2)$. The observation matrices $C(2)$, $C(3)$, and $C(4)$ are all selector matrices that only contains zeros and ones. The explicit expression of these observation matrices are omitted here.

ACKNOWLEDGMENT

The authors would like to thank the late research scientist at ERC, Dr. J. Yuan, who designed the testbed machining process and had many insightful discussions with the authors. They would also like to thank the anonymous reviewers for their enthusiastic efforts in the review process of this paper.

REFERENCES

- [1] R. Ramesh, M. A. Mannan, and A. N. Poo, "Error compensation in machine tools—a review part I: geometric, cutting-force induced and fixture dependent errors," *Int. J. Mach. Tools Manufact.*, vol. 40, pp. 1235–1256, 2000a.
- [2] ———, "Error compensation in machine tools—a review part II: thermal errors," *Int. J. Mach. Tools Manufact.*, vol. 40, pp. 1235–1256, 2000b.
- [3] R. Mantripragada and D. E. Whitney, "Modeling and controlling variation propagation in mechanical assemblies using state transition models," *IEEE Trans. Robot. Automat.*, vol. 15, pp. 124–140, 1999.
- [4] J. F. Lawless, R. J. Mackay, and J. A. Robinson, "Analysis of variation transmission in manufacturing processes—part I," *J. Quality Technol.*, vol. 31, no. 2, pp. 131–142, 1999.
- [5] R. Agrawal, J. F. Lawless, and R. J. Mackay, "Analysis of variation transmission in manufacturing processes—part II," *J. Quality Technol.*, vol. 31, no. 2, pp. 143–154, 1999.
- [6] J. Jin and J. Shi, "State space modeling of sheet metal assembly for dimensional control," *J. Manuf. Sci. Eng.*, vol. 121, pp. 756–762, Nov. 1999.
- [7] Q. Huang, J. Shi, and J. Yuan, "Part dimensional error and its propagation modeling in multi-operational machining processes," *J. Manuf. Sci. Eng.*, no. 125, May 2003.
- [8] D. Djurdjanovic and J. Ni, "Linear state space modeling of dimensional machining errors," *Trans. NAMRI/SME*, vol. XXIX, pp. 541–548, 2001.
- [9] R. P. Paul, *Robot Manipulators: Mathematics, Programming, and Control*. Cambridge, MA: MIT Press, 1981.
- [10] *Handbook of Geometrical Tolerancing: Design, Manufacturing and Inspection*, Wiley, New York, 1995.
- [11] A. Wirtz, C. Gachter, and D. Wipf, "From unambiguously defined geometry to the perfect quality control loop," *CIRP Ann. Manuf. Technol.*, vol. 42, no. 1, pp. 615–618, 1993.
- [12] H. Z. Yau, "Evaluation and uncertainty analysis of vectorial tolerances," *Precision Eng.*, vol. 20, pp. 123–137, 1997.
- [13] ———, "Generalization and evaluation of vectorial tolerances," *Int. J. PROD. RES.*, vol. 35, no. 6, pp. 1763–1783, 1997.
- [14] P. R. Kumar and P. Varaiya, *Stochastic Systems: Estimation, Identification, and Adaptive Control*. Englewood Cliffs, NJ: Prentice-Hall, 1986.

- [15] W. Cai, J. Hu, and J. Yuan, "A variational method of robust fixture configuration design for 3-D workpieces," *J. Manuf. Sci. Eng.*, vol. 119, pp. 593–602, Nov. 1997.
- [16] J. J. Craig, *Introduction to Robotics*. Boston, MA: Addison-Wesley, 1988.



Shiyu Zhou received the B.S. and M.S. degrees in mechanical engineering from the University of Science and Technology of China in 1993 and 1996, respectively, and the M.S. degree in industrial engineering and the Ph.D. degree in mechanical engineering from the University of Michigan, Ann Arbor, in 2000.

He is an Assistant Professor in the Department of Industrial Engineering at the University of Wisconsin-Madison. His research interests are the quality and productivity improvement methodologies by information integration based on control theory, advanced statistics, and engineering knowledge.

Dr. Zhou received Distinguished Achievements Award in 2000 at the University of Michigan. He is a member of IIE, INFORMS, ASME, and SME.



Qiang Huang received the B.S., M.S., and Ph.D. degrees in mechanical engineering from Shanghai Jiao-Tong University, Shanghai, China in 1993, 1996, and 1998, respectively. He is currently working toward the Ph.D. degree at the University of Michigan, Ann Arbor.

His research interests are centered on variation reduction for complex manufacturing processes, integrated design and manufacturing, and engineering statistics.

Dr. Huang is a member of ASME, INFORMS, IIE, and SME.



Jianjun Shi received the B.S. and M.S. degrees in electrical engineering from Beijing Institute of Technology in 1984 and 1987, respectively, and the Ph.D. degree in mechanical engineering from the University of Michigan, Ann Arbor, in 1992.

He currently is an Associate Professor in the Department of Industrial and Operations Engineering, University of Michigan. His research interests are the fusion of advanced statistics and engineering knowledge to develop in-process quality improvement (IPQI) methodologies achieving automatic process monitoring, diagnosis, compensation, and their implementation in various manufacturing processes. He received numerous awards and currently serves as a Department Editor of *IIE Transactions on Quality and Reliability*.

Dr. Shi is a member of ASME, ASQC, IIE, and SME.